Spring 2020

Using Surface-Enhanced Raman Scattering of Gold Nanostars for Encoding Molecular Information

Samantha E. Curry

USING SURFACE-ENHANCED RAMAN SCATTERING OF GOLD NANOSTARS FOR ENCODING MOLECULAR INFORMATION

By

Samantha Curry

A Thesis Submitted in Partial Fulfillment

Of the Requirements for the

University Honors Program

Department of Chemistry

The University of South Dakota

May 2020

The members of the Honors Thesis Committee appointed

to examine the thesis of Samantha Curry

find it satisfactory and recommend that it be accepted.

DocuSigned by:
Chaoyang Jiang
2171313D0259446...
6/3/2020

Dr. Chaoyang Jiang

Associate Professor of Chemistry

Director of the Committee

DocuSigned by:
Miles Koppang
F1333D14D2DF41B...
6/3/2020

Dr. Miles Koppang

Professor of Chemistry

DocuSigned by:
David C Hawkinson 6/3/2020
35D954DE9CB6410...

Dr. David Hawkinson

Associate Professor of Chemistry

ABSTRACT

Using Surface-Enhanced Raman Scattering of Gold Nanostars for Encoding Molecular Information

Samantha Curry

Director: Chaoyang Jiang, Ph.D.

Increases in the selling of illicit goods warrant a subsequent need for even more sophisticated methods to prevent counterfeit products from being sold. Surface-enhanced Raman spectroscopy (SERS) has the potential to be a powerful tool to thwart counterfeiters because the unique security tags fabricated with this method are difficult to reproduce without knowing the "secret" recipes used in their preparation. In this work, gold nanostars are used as SERS active substrates since their branched structure allows for strong coupling between the light and plasmonic nanoparticles. As a result, Raman signals of trace amount of chemicals can be easily detected. The gold nanostars were used with different combinations of probe molecules so that unique anti-counterfeiting tags can be created. The reproducibility and uniformity of the SERS spectra for these tags were analyzed using principal component analysis (PCA). These SERS tags have a great potential for a variety of anti-counterfeiting applications.

Keywords: Raman, SERS, gold nanostars, anti-counterfeiting

Table of Contents

List of Figures

List of Tables

ACKNOWLEDGEMENTS

I would like to thank the National Science Foundation REU program (NSF REU site: Security Printing and Anti-Counterfeiting Technology Grant EEC-1560323) for funding this research. NSF MRI program (CHE-1337707) for the SEM that was used in this project. I would also like to thank Dr. Aravind Baride for the help with the SEM imaging. The Raman spectrometer used was funded by the Surface Engineering Research Center (SERC) by the state of South Dakota, Governor's Office of Economic Development. Lastly, I would like to thank the CY research group and the University of South Dakota Department of Chemistry for the continual support throughout this project, particularly Dr. Chaoyang Jiang and Yifeng Huo for kindly mentoring me throughout my undergraduate research career.

CHAPTER ONE

1 Introduction

1.1 Counterfeiting and the Importance of Anti-Counterfeiting Technology

The sales of illicit goods are an increasing problem for consumers, governments, and businesses around the world leading to devasting effects on the economy and consumer health. Governments and businesses have spent a significant amount of time, money, and energy to protect their products from counterfeiting and other intellectual property infringements.[1, 2] While counterfeiting is not a new concept, it has only become a significant problem around the world recently.[1] In 2017 the global anti-counterfeiting technology market was $51.8 billion and is projected to reach $208.4 billion by 2023.[3]

One area where counterfeiting is especially dangerous to consumers is medical counterfeiting. The World Health Organization defines medical counterfeiting as "deliberately and fraudulently mislabeled with respect to identity or source". Drugs that are the most at risk of being fraudulent tend to be life-saving or expensive medications. Counterfeit medications often contain none or very little of the active ingredients, making them directly harmful to consumers. These products also tend to contain harmful compounds like floor wax or carcinogens. Illicit medications pose a serious risk to consumer health as also attribute to the economic impact of counterfeiting.[4]

Another sector that experiences a significant amount of counterfeiting that can be dangerous to consumers is electronic components and systems. Counterfeit electronics can pose health risks by being defective, purposely tampered with, or unreliable.[5] These products can also threaten national security. Counterfeit products have been detected in the U.S. Department of Defense supply chains, including memory devices in missile systems. This may cause susceptibility to security breaches or critical loss of system function, which could have dangerous consequences.[6] Counterfeiting can have widespread effects, including detrimental effects to national security.

New and complex innovations in anti-counterfeiting technology are necessary to prevent the growing issue of illicit sales. Without intervention, counterfeit products will continue to threaten the economy, the lives of consumers, and national security. Herein, we propose a method for developing an anti-counterfeiting technology that is complex enough to prevent counterfeiters from duplicating it while being reproducible for large-scale application.

1.2 Approaches to Anti-Counterfeiting

The most popular anti-counterfeiting methods are based on luminescent materials that emit light under excitation to revel different colors. These technologies rely on luminescent materials such as lanthanide nanomaterials, quantum dots, and metal-organic framewords.[7]

In 2018, Kalytchuk et al., published a paper where they used carbon dots to fabricate invisible luminescent tags for anti-counterfeiting applications.[8] This group's method combined the fluorescent properties of carbon dots with distinct fluorescent

lifetimes to yield two types of carbon dot fluorescent inks with identical emission but different lifetimes. Figure 1.1 shows the mechanism of Kalytchuk et al.'s anti-counterfeiting tags where (a) is the tag under UV light and (b) is the same tag and the lifetimes have been colored. They also showed that carbon dot tags could be incorporated into inks for practical application.[8]

Another anti-counterfeiting technique takes advantage of the infrared (IR) emissions from silver nanowire (AgNW) films. In a 2020 paper, Wang et al. showed that ultrathin AgNW films are nearly invisible to the naked eye and visible when using an IR camera.[7] They spray coated the films onto surfaces to create different patterns and the brightness varies with AgNW loading density. Figure 1.2 shows a star-shaped pattern and the results indicated that increasing brightness with increasing loading density.[7]

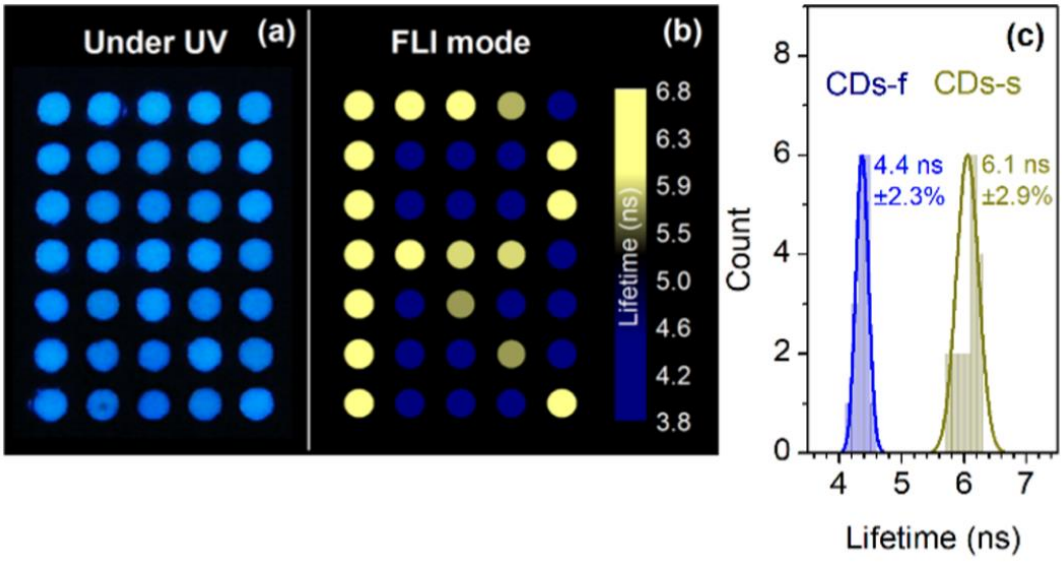

Figure 1.1 (a) Anti-counterfeiting tag photographed under UV light, (b) the same tag using pseudo-colors to indicate the fluorescent lifetime of each pixel, and (c) fluorescent lifetime histogram obtained from the pixels. Image reprinted with permission from *ACS Appl. Mater. Interfaces*. **2018**, 10, 35, 29902-29908.[8]

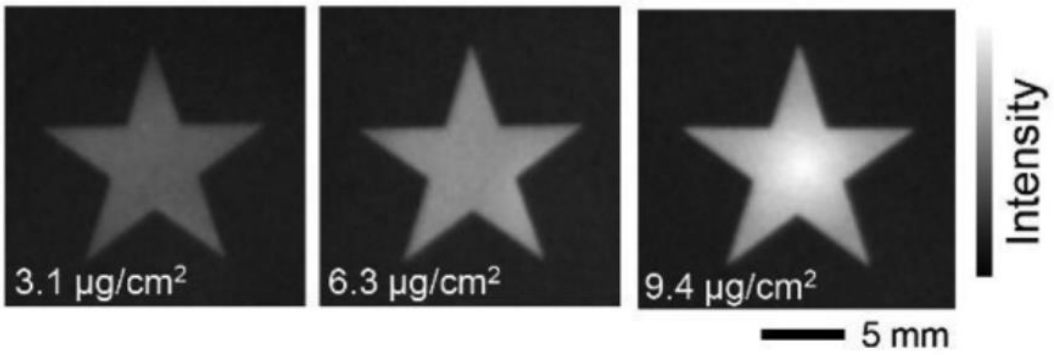

Figure 1.2 Spray coated AgNW films used to create a star-shaped pattern showing that increasing AgNW loading density corresponds to increasing image brightness. Image reprinted with permission from *J. Materiomics.* **2020** 6 (1), 152-157.[7]

Using fluorescent materials are capable of creating anti-counterfeiting tags, but these are limited in their information capacity. Anti-counterfeiting techniques based in these methods are also more easily copied by counterfeiters, making them less secure. Anti-counterfeiting tags that utilize SERS are more difficult to counterfeit and have a high capacity for information.

1.3 Applications of SERS in Anti-Counterfeiting

Raman scattering consists of inelastic light scattering in which the scattered radiation carries vibrational information that is unique to the corresponding molecular structure. This phenomenon was first observed in 1928 by Sir Chandrasekhara Venkata Raman. He was awarded the 1930 Nobel Prize in Physics for his work on Raman scattering.[9] There are two types of Raman scattering, Stokes and anti-Stokes. In Stokes Raman scattering the molecule shifts from its ground state to a virtual energy state and then

to an excited vibrational energy state and the photons energy decreases. In anti-Stokes Raman scattering, the molecule shifts from an excited vibrational state to a virtual state, then relaxes to its ground state. In this case, the photons energy increases. The possibilities of light scattering are shown in Figure 1.3.

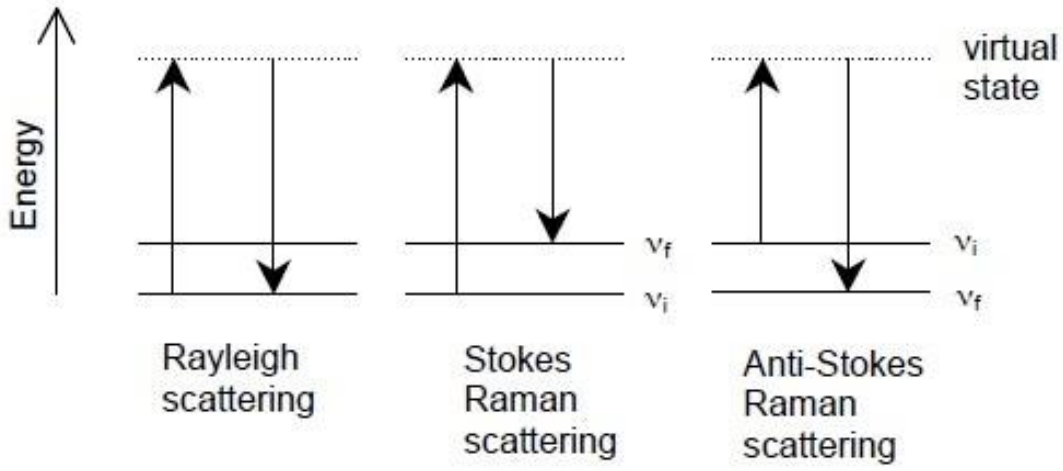

Figure 1.3 Diagram showing the mechanism of the different types of light scattering: Rayleigh, Stokes Raman, and anti-Stokes Raman.

Raman signals are very useful in understanding chemical binding structure, but the main disadvantage in the application of Raman scattering is its inherently weak signal intensities. However, Raman signals can be greatly enhanced by attaching the probe molecules to the surface of certain materials in a process called surface-enhanced Raman scattering (SERS). These materials often consist of precious metals such as gold or silver. Since the discovery of SERS in 1974 by Fleischmann while working with pyridine adsorbed onto a roughened silver electrode, many advancements have been made.[10] Recently, SERS has been shown to be powerful enough to detect single molecules.[11]

The SERS substrate chosen for this study was gold nanostars (AuNS) due to their highly branched structure. The enhancement on the surface of a plasmonic substrate, such

as AuNS, is concentrated at regions called “hot spots”. These hot spots are often found in nanogaps between nanoparticles or at sharp tips.[10] Figure 1.4 shows hot spots created in the gaps between two gold nanospheres and two gold nanocubes. The enhancement in these gaps were found to be 10^4 times higher than the enhancement on the surface of a single nanostructure.[12] Coupled nanostructures provide electromagnetic field enhancements that originate from the excitement of surface plasmons that induce amplification of laser light in small spatial regions, causing stronger signal enhancements than isolated nanostructures.[10, 12]

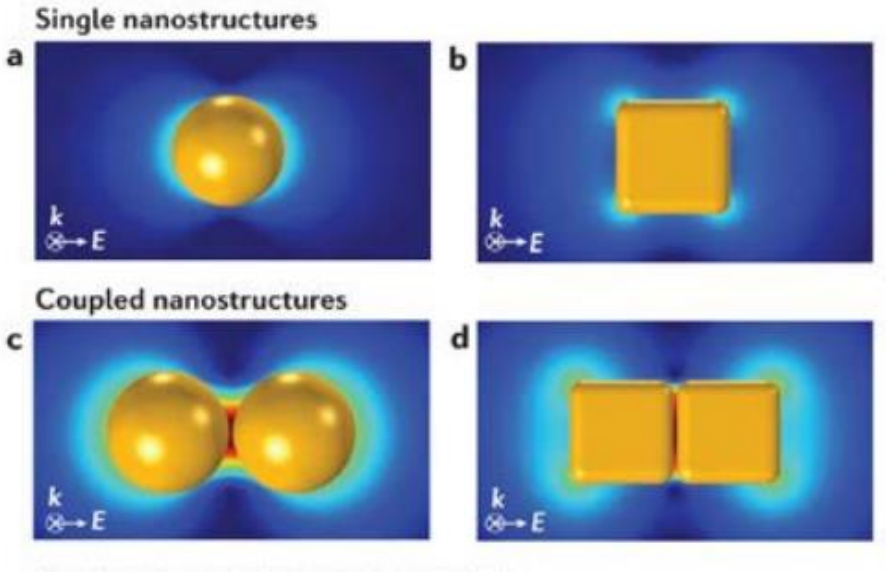

Figure 1.4 Simulated surface enhancement of (a) a single nanosphere, (b) a single nanocube, (c) coupled nanospheres, and (d) coupled nanocubes. Image reprinted with permission from *Nat. Rev. Mater*. **2016**, 1, 16021.[12]

One example of using SERS in anti-counterfeiting technology is a 3D SERS encoding system proposed by Liu et al. in 2017.[13] By fabricating plasmonic candlestick microstructures with differing heights, the z-direction can be utilized, and more complex

security labels can be created. Multiple layers of images were able to be encrypted into 3D candlestick microstructure arrays, as shown in Figure 1.5. These images were able to be revealed using SERS images acquired at specific z values. This study used only one probe molecule, meaning that the encoding capacity of this method could be greatly increased by incorporating more probe molecules.[13]

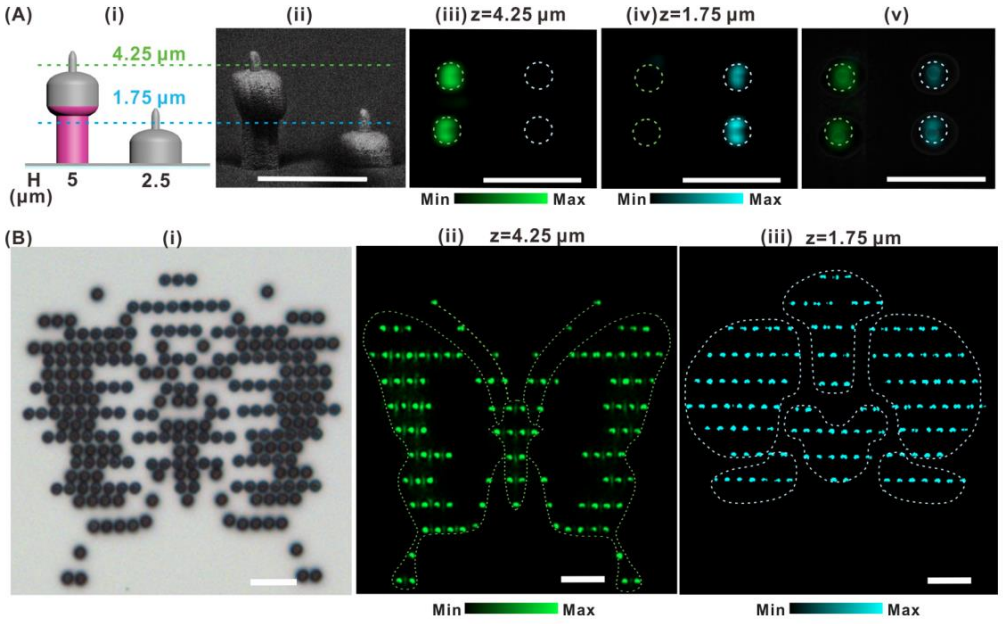

Figure 1.5 3D SERS anti-counterfeiting security labels. (A) (i) schematic of the labels, (ii) side-view SEM image with SERS focal planes of (iii) z=4.25 µm and (iv) z=1.75 µm. (v) SERS images overlaid on a top-down SEM view. Scale bars are 5 µm. (B) (i) optical microscope image with x-y SERS images acquired at focal planes of (ii) z=4.25 µm and (iii) z=1.75 µm. The orchid and butterfly shapes were constructed using 2.5 and 5.0 µm candlestick microstructures, respectively. Scale bars are 10 µm. Image reprinted with permission from *ACS Photonics.* **2017**, 4 (10), 2529-2536.[13]

Aside from their applications in anti-counterfeiting technology, AuNS have also been applied in catalysis[14, 15], photothermal therapy[16, 17], biosensing[18, 19], and bioimaging[20].

The various different applications of AuNS are due to their unique characteristics and morphology. Their highly branched structure allows for increased surface area which is useful in catalytic applications and transforming photon energy into heat for photothermal applications.[21] AuNS also exhibit significant SERS enhancement, making them even more applicable in practical applications.

1.4 Our Approach

There is a growing need for more sophisticated anti-counterfeiting technologies. We believe that SERS is an effective method for the creation of novel anti-counterfeiting technologies due to the vibration fingerprints of molecules, simultaneous detection of different analytes, portability of instruments, and high sensitivity of SERS.[10]

Previous research in our group has yielded an effective method for the synthesis of gold nanostars using a seed-mediated growth mechanism.[22] Dr. Meng studied the growth of the AuNS through the variation of experimental parameters and found that hydroquinone and 4-mercaptobenzoic acid are necessary for the growth and stabilization of the branches. She also showed that the AuNS exhibit strong enhancement of SERS signals.[23]

In this work, AuNS were synthesized using Meng's approach were combined with a variety of probe molecules to fabricate anti-counterfeiting tags. The probe molecules were encoded into a binary number system and were able to be decoded using Raman spectroscopy and principle component analysis (PCA). With improvements to their stability and information capacity, the SERS tagging method show promise to be an effective approach to enhance security measures and prevent counterfeiting.

CHAPTER TWO

2 Materials and Methods

2.1 Chemicals and Preparations

Gold chloride solution ($HAuCl_4 \cdot 3H_2O$, 30 wt %) and melamine were purchased from Sigma Aldrich (MO, USA). Trisodium citrate dihydrate, L-(+)-ascorbic acid, and methylene blue (MB) were purchased from Alfa Aesar (MA, USA). Hydroquinone (HQ), rhodamine 6G (R6G), crystal violet (CV), 4-aminothiolphenol (4-ATP), 4-mercaptopyridine (4-MPy), and hydrogen peroxide (30 wt %) were purchased from Acros Organics (NJ, USA). 4-mercaptobenzoic acid (4-MBA) was purchased from TCI America (OR, USA). Malachite green (MG), sulfuric acid (96%), hydrochloric acid (37%), and nitric acid (69%) were purchased from Thermo Fisher Scientific (MA, USA). Anhydrous ethanol was purchased from Pharmco-AAEPR (CT, USA). Nochromix powders were purchased from Godax Laboratories (MD, USA). Chemicals were all utilized without further purification.

Nanopure water (18.2 MΩ·cm) was used for the cleaning and the preparation of aqueous solutions. All of the glassware used in these experiments were cleaned prior to use. Flasks and vials were soaked in a Nochromix bath for one day, then rinsed with thoroughly nanopore water and dried in an oven at 100 ºC before use. The bath was prepared by adding one package of Nochromix powder to 5 L of 96% sulfuric acid.

2.2 Materials Synthesis

The gold seed solution (13 nm gold nanoparticles) was prepared using a citrate reduction method reported by Frens.[24, 25] This was performed in a three-neck round-bottom flask. The flask was treated with fresh aqua regia solution and thoroughly rinsed prior to use. The aqua regia solution consisted of 37% hydrochloric acid and 69% nitric acid mixed in a 3 to 1 ratio. Once the flask was prepared, the $HAuCl_4$ stock solution was diluted to make 50 mL of 1 mM solution. This solution was boiled with stirring and a condenser is used for refluxing. Then, 5 mL of 38.8 mM sodium citrate solution was injected quickly into the boiling solution. After this addition, the solution changed color from light yellow to dark red. The boiling was continued for 10 minutes, then the mixture was allowed to cool to room temperature. The gold seed solution was stored in the flask and used in the synthesis of the gold nanostars.

Gold nanostars were synthesized using a modified version of a method previously reported by our group.[22, 23] To begin, 23 mL of nanopore water was added to a flask. While stirring, 1 mL of 10 mM $HAuCl_4$, 200 µL of the previously prepared gold see solution, 200 µL 0.2 wt % sodium citrate, 400 µL of 100 mM HQ, and 200 µL of 1 mM 4-MBA were added in that order. After adding the HQ to the mixture, the solution color changed to a dark purple.

To prepare the tag solutions, nine chemicals were used to create a system of encoded chemical combinations. Nine different probe molecules were selected for this study: 4-MBA, R6G, MB, CV, melamine, 4-ATP, 4-MPy, and ethanol. Ethanol acts as both a SERS-sensitive material and as a cosolvent. To encode these chemicals, each one was treated as a digit in binary code with 1 representing its presence and 0 representing its

absence. Therefore, by using nine different molecules 2^9 combinations are possible. A random number generator was used to select the eight tags used in this study. Each tag solution was prepared by mixing each of the necessary stock solutions so that a final concentration of 100 µM was achieved. To produce the tags, 100 µL of the tag solution mixture was added to 900 µL of AuNS solution. These tags were then ready for further experiments.

2.3 Characterizations

A Cary 50 Bio Spectrophotometer (Varian Inc., Palo Alto, CA, USA) and a GENESYS 30 Visible Spectrophotometer (Thermo Fisher Scientific Inc., Waltham, MA, USA) were used to obtain UV-Vis spectra of the gold seed and AuNS solutions. Nanopure water was used for background correction for all measurements in this study. The sample container was a quartz cuvette with a 1 cm beam path for the Cary 50 spectrophotometer and a 25 mm diameter cylindrical glass vial was used for the GENESYS 30 spectrophotometer. Cuvettes were cleaned using aqua regia while the vials were cleaned using Nochromix solution. The scanning speed of the Cary 50 spectrophotometer was set to 1 nm/s.

The morphologies of the gold seed and AuNS were examined using scanning electron microscopy (SEM). A field SEM (Zeiss, Pleasanton, CA, USA) was used for this investigation with an acceleration voltage of 4.0 kV and working distance of 4.1 mm. Silicon slides were used as the substrates for SEM analysis. These were cut into 1 cm by 1.5 cm rectangles and cleaned using piranha solution, prepared with 96% sulfuric acid and 30% H_2O_2 solution in a 3 to 1 ratio. After 30 minutes of immersion in the piranha solution,

the slides were rinsed using nanopore water and stored in vials containing nanopore water. Prior to use, the slides were dried using nitrogen gas. Samples were prepared using 1 mL of colloidal solution. The solutions were centrifuged for 5 min at 10000 rpm and the supernatants were removed. 10 µL of the remaining solution were dropped onto a silicon slide and dried at room temperature, then further dried under vacuum at 16 kPa of pressure overnight.

An i-Raman EX portable Raman Spectrometer (B&W Tek, Inc., Newark, DE, USA) was used to obtain Raman spectra of our samples using a sample holder for glass vials (Fisherbrand, 03-338A). The excitation wavelength was 1064 nm with a power of 350 mW. Acquisition time varied between 1 s to 5 min, depending on the sample. Background signals were removed using dark corrections.

SERS spectra were analyzed using principle component analysis (PCA). In Origin 2018 software (OriginLab Corp., Northampton, MA, USA), a function called PCA for spectroscopy (OriginLab Technical Support, V1.0) was used. In order to perform PCA, 5 spectra of each sampled needed to be acquired. These spectra were processed prior to PCA. In the software, each sample's spectra were grouped into a batch. A 95% confidence interval for the batch is calculated by the software and indicated as an ellipsis while each spectrum is plotted as a point. The ellipses and points are used to indicate whether samples and batches are related or significantly different from one another.

CHAPTER THREE

3 Results and Discussion

3.1 UV-Vis Spectra

Gold nanoparticle and AuNS solutions have different colors and therefore different extinction spectra. The spectra for both the gold seed solution and the AuNS solution are shown in Figure 3.1. The maximum absorbance of the AuNS solution is at 606 nm and 520 nm for the gold seed solution. These peaks can be used to roughly determine the sizes of the particles while the width of the peak can give an indication of particle uniformity. However, it is difficult to exactly determine these characteristics for the AuNS due to the number of additional factors involved. The peak that is present at 875 nm in the AuNS spectra that is not present in the gold seed spectra is an indication of particle aggregation. The decreased stability of the AuNS may be due to the addition of other molecules such as ethanol.

To determine the optimum concentration of gold seed solution to form AuNS, four different batches were prepared. These batches contained 2 mL, 1 mL, 0.5 mL, and 0.2 mL of gold seed, respectively and their UV-vis spectra can be seen in Figure 3.2. The colors of the solutions are shown in the figure insert. The total added volume for each of these measurements was 2 mL, with nanopore water accounting for the additional volume. When using 0.2 mL a large aggregation peak is observed, meaning that this amount of gold seed leads to AuNS with low stability and are not appropriate for this study. The peak positions of the different AuNS solutions give an indication of the size of the particles.

Based on the spectra, the AuNS that were prepared with less seed solution are larger. Since there was less seed solution, each AuNS was able to grow more than if there is more seed solution present. Based on the observed spectra, the seed concentration that was chosen for this study was 1 mL. This is due to the relatively low intensity of the aggregation peak compared to the other volumes and the sizes of the resulting particles.

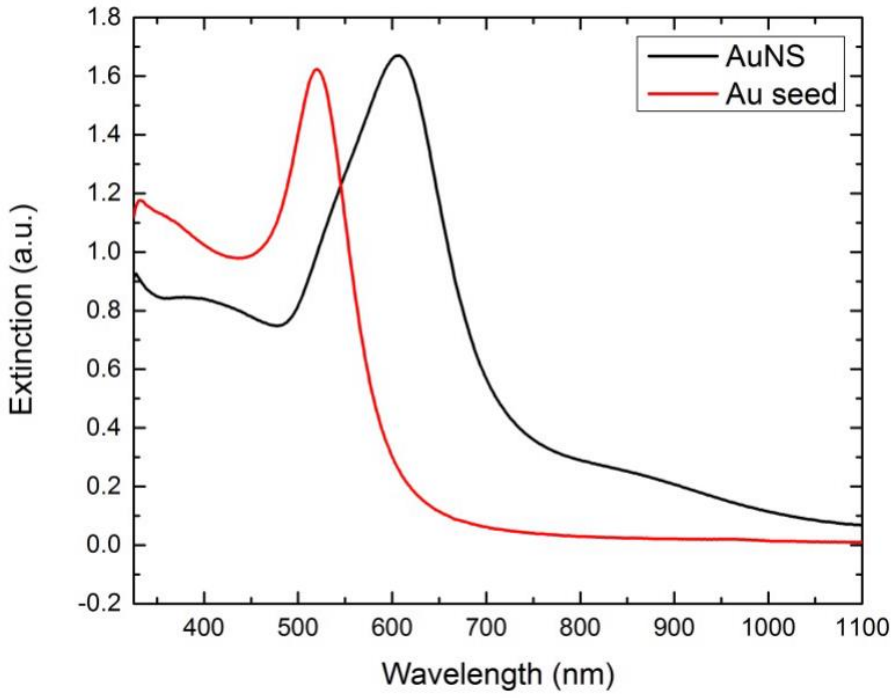

Figure 3.1 UV-Vis spectra of AuNS and gold seed solutions scanned from 1100-325 nm.

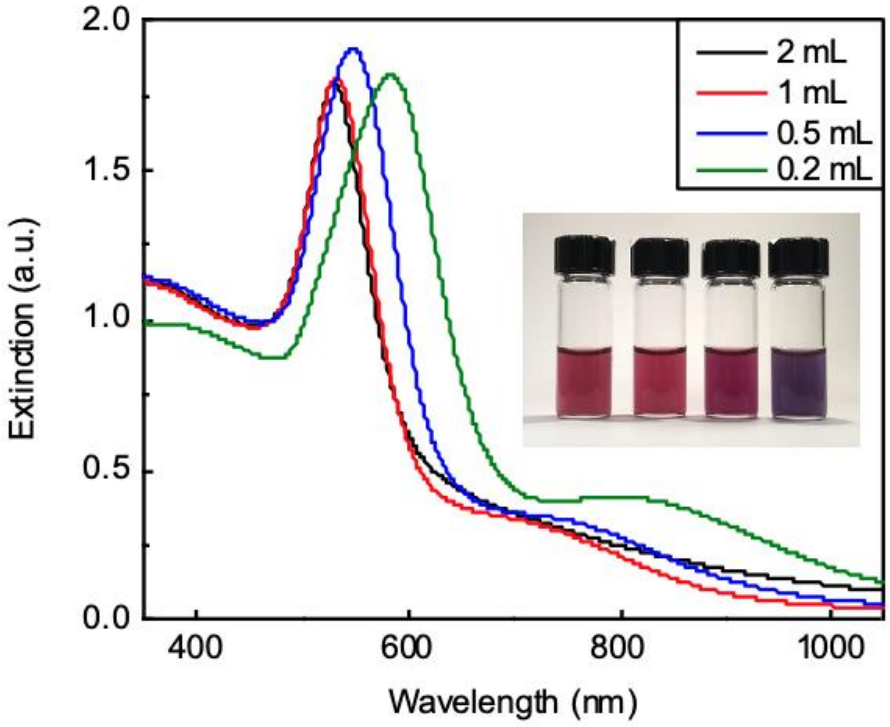

Figure 3.2 UV-Vis spectra of AuNS solutions prepared with 2 mL (black), 1 mL (red), 0.5 mL (blue), and 0.2 mL (green) gold seed solution. In the inserted figure, the volume of gold seed solution used from left to right is 2 mL, 1 mL, 0.5 mL, and 0.2 mL.

3.2 Morphology Characterization

SEM imaging was used to determine the morphologies of AuNS. In Figure 3.3, the SE2 probe was used at 10k magnification. Figure 3.4 also uses the SE2 probe, but at 100k magnification. Both images use a 4.1 mm working distance and 4 kV acceleration voltage. At 25k magnification, the relative uniformity of the nanostars can be observed.

When using 100k magnification, the branched structures of the AuNS are better observed. Although the AuNS are not exactly identical, all of the nanostars have branches with similar length and structure. The non-uniformity most likely originates from an

uneven distribution of HQ and 4-MBA in the star synthesis process. The AuNS are on average about 60 nm in length.

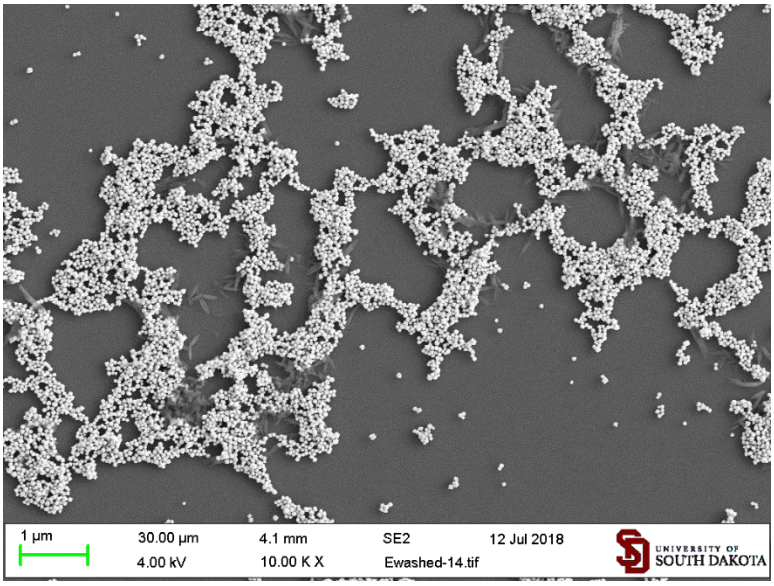

Figure 3.3 SEM image of AuNS taken at 10k magnification.

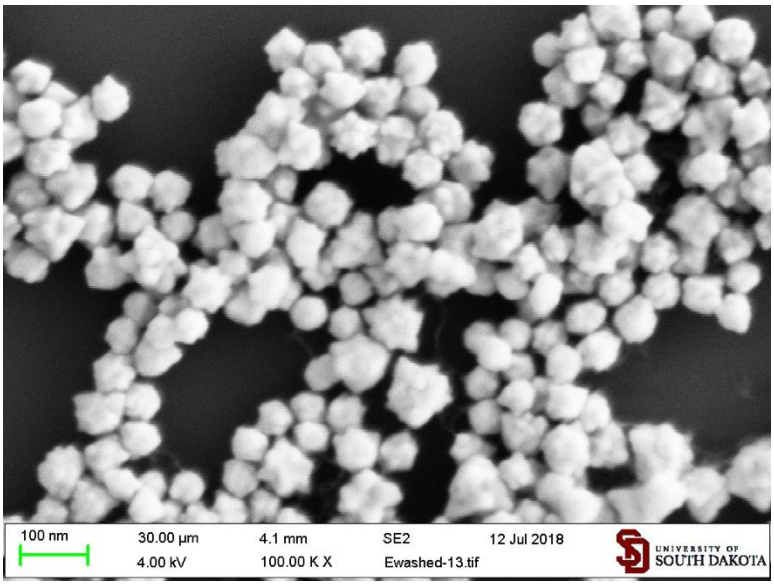

Figure 3.4 SEM image of AuNS taken at 100k magnification.

3.3 Comparison to Spherical Gold Nanoparticles

To show that AuNS have a greater SERS enhancement and therefore are better suited for this research, a batch of gold nanospheres were synthesized for comparison. The gold nanospheres were of similar size to the AuNS and were synthesized using the same method as the AuNS, except that 4-MBA was added one hour after the addition of HQ. Other than this, the concentrations and experimental procedure for the spherical gold nanoparticles was the same as that for the AuNS.

After the addition of HQ, the gold nanosphere solution turned dark blue, but faded into a purple color. The observed color change is likely due to the branched particles relaxing into spheres.[22] There were no further color change observed, even after the addition of 4-MBA. The sharp branches of the AuNS have begun to relax back into a spherical shape.

The color difference between the AuNS and the spherical particles was indicated using UV-Vis. The spectra of both particles are shown in Figure 3.5. The SPR peak for the gold nanosphere solution was determined to be at 543 nm and 606 nm for the AuNS. This shows that there is a size difference between the two different particle shapes, likely due to the shrinking of the branches as the star shaped particle evolves into a spherical shape. The lower intensity and broadness of the AuNS compared to the spherical gold nanoparticles shows that there is a larger distribution in sizes between the AuNS.

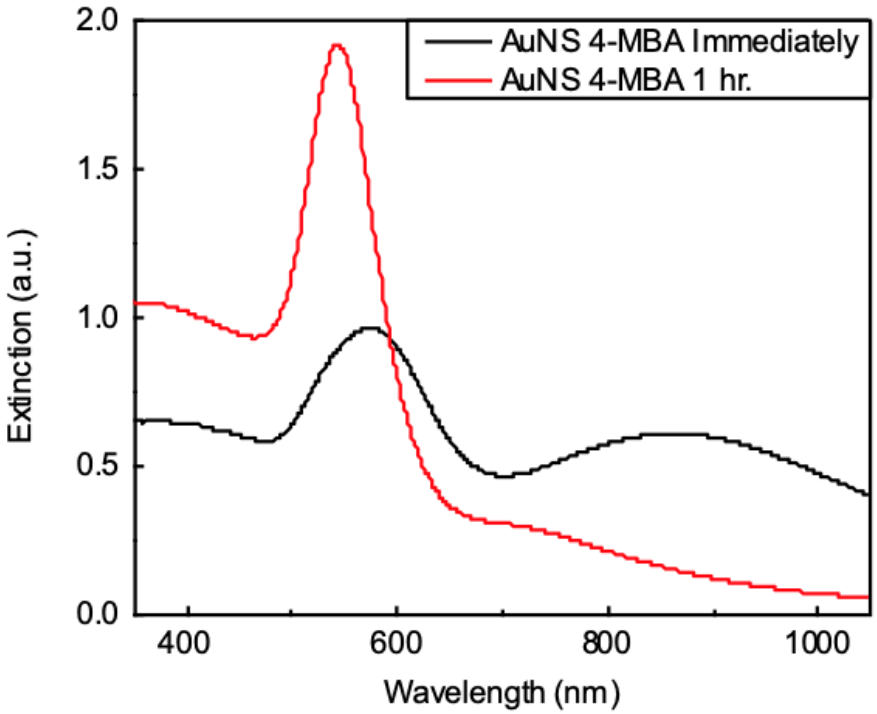

Figure 3.5 UV-Vis extinction spectra comparing gold nanospheres (black) with AuNS (red) scanned between 325 and 1100 nm with default scanning speed. Both solutions needed to be diluted to half of their original concentration using nanopore water.

The morphology of the nanospheres were investigated using SEM. The preparation method for the gold nanospheres is the same as was used for the AuNS for SEM imaging. Figure 3.6 was taken using a lower magnification, 100k, and the InLens probe whereas Figure 3.7 was taken at a higher magnification, 250k, and using the SE2 probe. These images show that the shape of the particles is not exactly spherical. The non-uniform shape of these particles may be due to incomplete relaxation caused by the addition of 4-MBA.

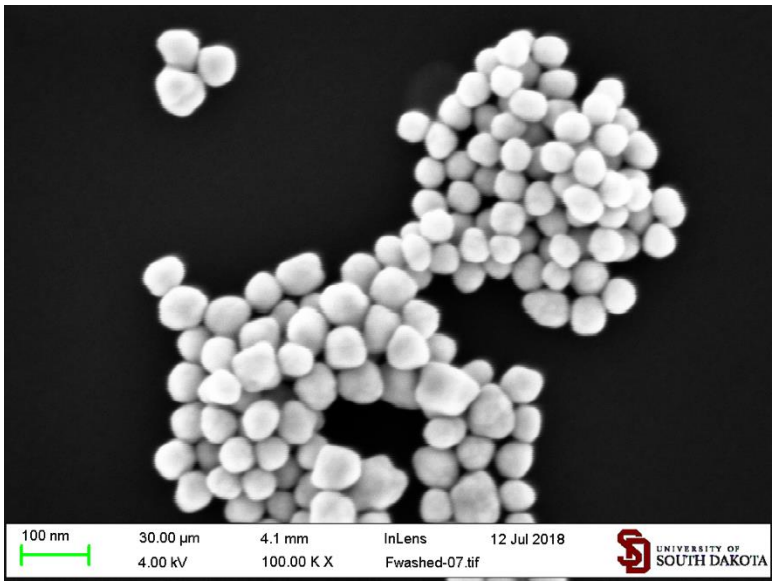

Figure 3.6 SEM image of gold nanospheres taken at 100k magnification.

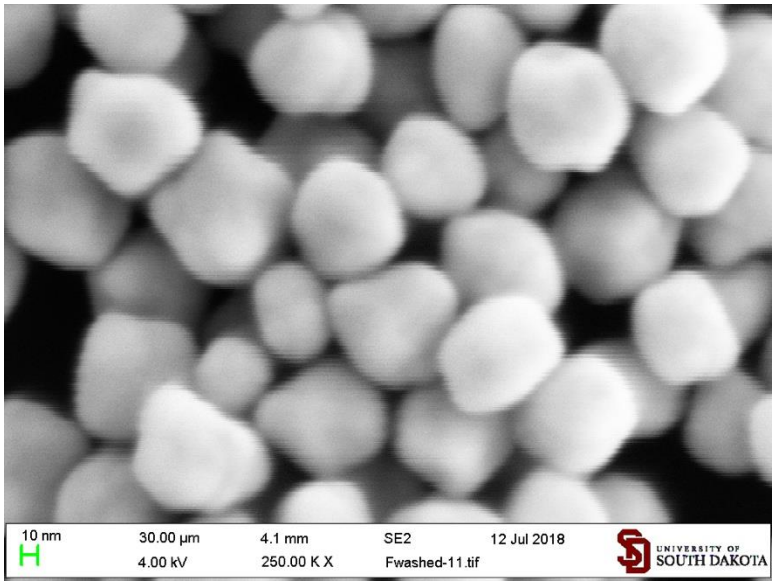

Figure 3.7 SEM image of gold nanospheres taken at 250k magnification.

To compare the SERS enhancement of the AuNS and the spherical gold nanoparticles, Raman spectra of each with the addition of a single probe molecule were compared. 5 µL of 100 nM R6G was added to both 1 mL of AuNS and 1 mL of gold

nanospheres. This resulted in a final concentration of 0.5 nM R6G in both samples. Even though the R6G peak is not observed due to its low concentration, the Raman spectra were unique enough to be distinguished by the PCA software. Raman spectra were taken the unaltered AuNS and gold nanosphere solutions along with those with the added R6G. These spectra were measured using 1 s exposure time and a 1064 nm laser.

From the Raman spectra shown in Figure 3.8, an increased in peak intensity is observed in the AuNS samples when compared with the gold nanosphere samples. These peaks are associated with the freezing agent, 4-MBA and the increased intensity may be due to the "hot spots" created by the branches or the increased surface area of the AuNS. The spectra were also analyzed using PCA and the score plot is found in Figure 3.9. The 95% confidence ellipses for the gold nanospheres and the gold nanospheres with the added R6G are not able to be separated and are therefore not able to be distinguished. The AuNS and AuNS with the added R6G are able to be separated. This means that these samples can be distinguished by the PCA software. The enhancement of the R6G peaks by the AuNS is greater than that of the gold nanospheres, which leads to the separation of the 95% confidence intervals. This shows that AuNS possess a greater ability to increase SERS signals than gold nanospheres and are a more appropriate choice for the fabrication of anti-counterfeiting tags.

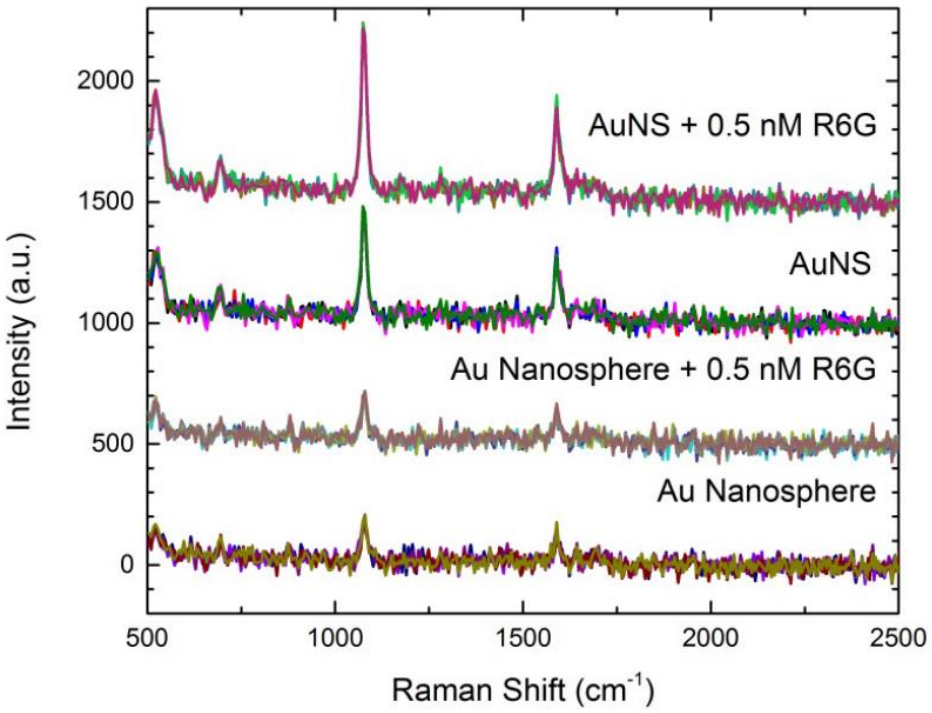

Figure 3.8 SERS spectra of gold nanospheres, gold nanospheres with 0.5 nM R6G, AuNS, and AuNS with 0.5 nM R6G using a 1064 nm laser and 1 s exposure time for each measurement. Each sample was measure 5 times so that PCA could be performed.

The SERS enhancement factor of the AuNS was determined by comparing the Raman spectrum of a 10% ethanol solution to that of 1 mL of AuNS solution with 10% ethanol. The enhancement factor of the AuNS was determined to be ~3,900. This number is not ideal when compared to the much higher enhancement factors that other groups have reported, but it does show that the AuNS are able to achieve high Raman signal intensities. High signal intensities are necessary for fabricating SERS anti-counterfeiting tags.

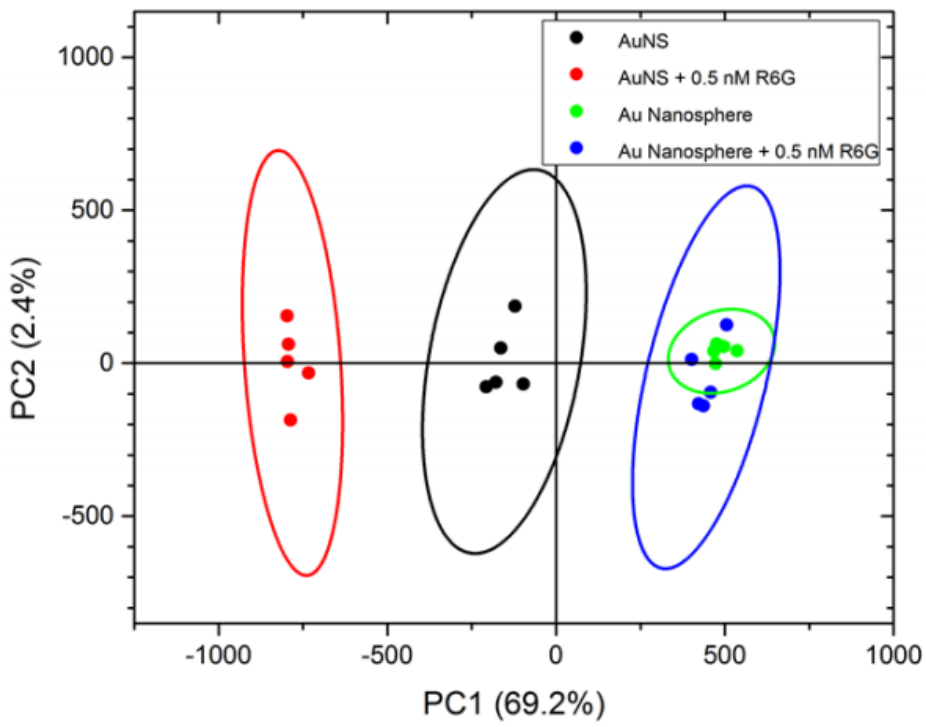

Figure 3.9 PCA score plot of the SERS spectra measured for the gold nanospheres (green), gold nanospheres with 0.5 nM R6G (blue), AuNS (black), and AuNS with 0.5 nM R6G (red).

3.4 Anti-Counterfeiting Tag Fabrication

To select our probe molecules for this study, we looked for molecules with high Raman cross sections and strong interactions with the AuNS, like those with thiol groups and without negative charges. We also searched for a variety of functional groups so that the SERS spectra of the molecules would be more varied and more easily distinguished. From these criteria, nine probe molecules were selected: 4-MBA, R6G, MB, CV, melamine, 4-ATP, 4-MPy, ethanol, and MG. The structures of the chosen molecules are shown in Figure 3.10.

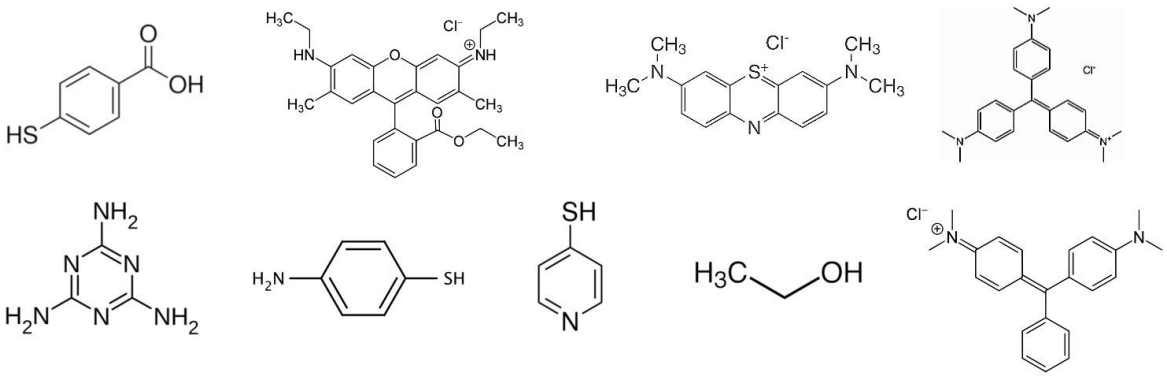

Figure 3.10 Chemical structures of each of the nine Raman probe molecules that were selected for these experiments.

The SERS spectra of each of the individual molecules are shown in Figure 3.11. These were acquired by using AuNS and 1 mM concentration of the probe molecule, except for ethanol. For ethanol, a 1:2 volume ratio of ethanol to AuNS solution was used. The exposure time used to acquire these spectra was 5 s and each was normalized. From the spectra, it is shown that the addition of each molecule creates a unique SERS spectrum.

The random numbers that were chosen for this experiment were 148, 100, 242, 73, 127, and 8. These were chosen from a random number generated with the criteria that they ranged from 0-512. Since we selected eight probe molecules, the number of possible combinations was 256, based on the following equation:

$$p = 2^n$$

Where p is the total number of possible outcomes and n is the number of probe molecules. The codes for these tags are shown in Table 3.1. In this encoding method, a "1" in the table indicates that the specified probe molecule is present with a concentration of 100 μM and a "0" indicates that it is absent.

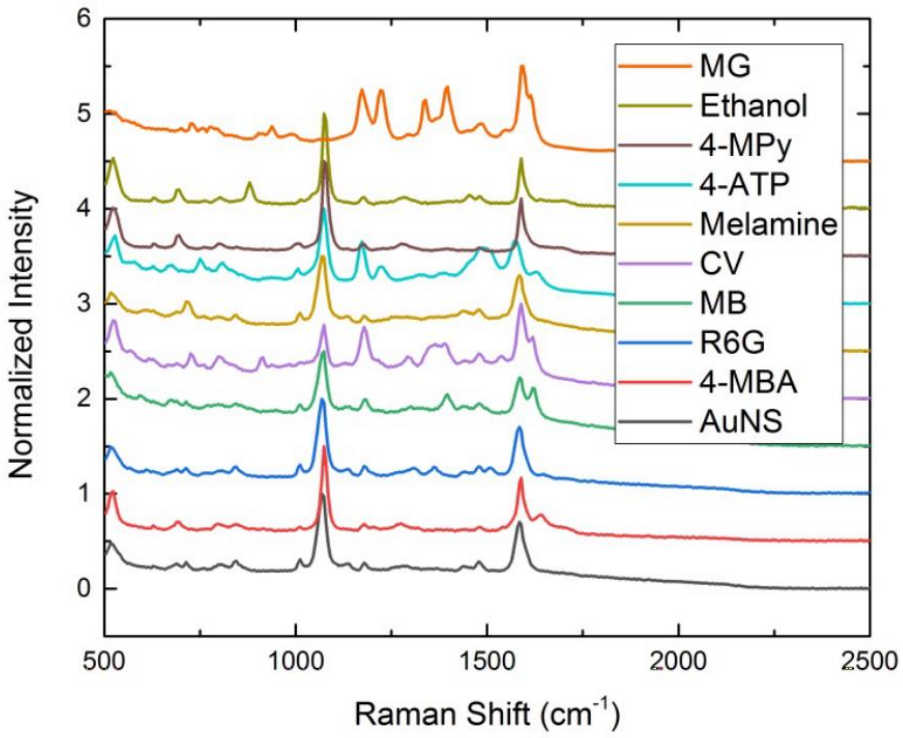

Figure 3.11 Normalized SERS for each of the Raman probe molecules using AuNS for the surface enhancement and the SERS spectra of the unaltered AuNS solution using a 1064 laser excitation and 5 s exposure time.

Table 3.1 Probe molecule encoding of each of the tag solutions using binary code.

Molecules	**4-MBA**	**R6G**	**MB**	**CV**	**Melamine**	**4-ATP**	**4-MPy**	**Ethanol**	
Tag I	1	0	0	1	0	1	0	0	148
Tag II	0	1	1	0	0	1	0	0	100
Tag III	1	1	1	1	0	0	1	0	242
Tag IV	0	1	0	0	1	0	0	1	73
Tag V	0	1	1	1	1	1	1	1	127
Tag VI	0	0	0	0	1	0	0	0	8

SERS spectrum of each tag were measured with an exposure time of 1 s and are shown in Figure 3.12. The relatively large peaks at 1076 cm^{-1} and 1585 cm^{-1} are due to the 4-MBA that was used in the synthesis process. The PCA score plots of these spectra are shown in Figure 3.13. Since each of the tag solutions are able to be separated from by the PCA software, we can conclude that the method has the ability to be used to create unique and differentiable anti-counterfeiting tags. The small ellipse size indicates that the spectra measurements of the tags are highly reproducible. Before the tags can be implemented into commercial or industrial settings, their stability and information capacity must be further improved.

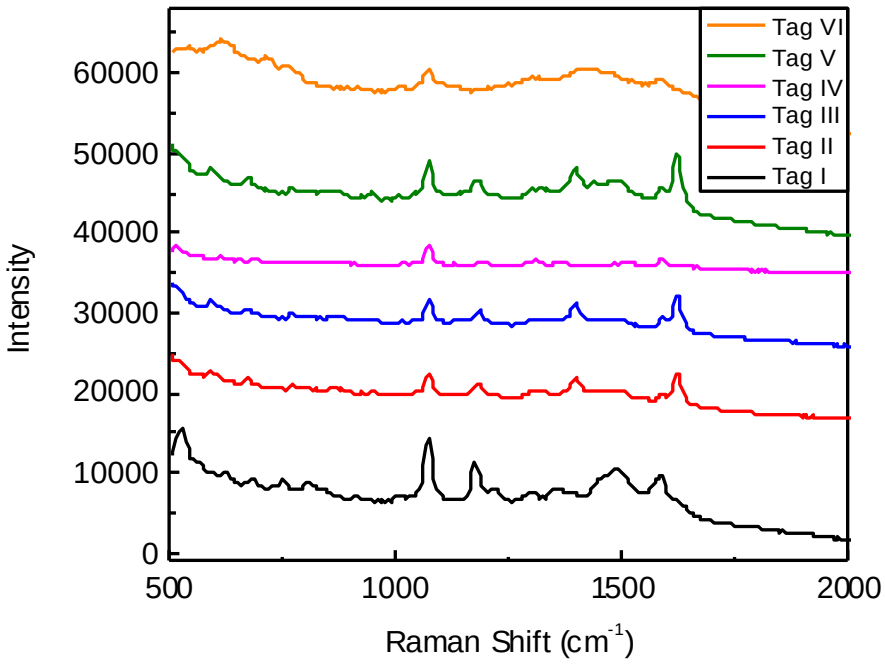

Figure 3.12 Normalized SERS spectra of each of the six tags chosen from a random number generator and the SERS spectrum of the AuNS using a 1064 nm laser excitation and a 1 s exposure time.

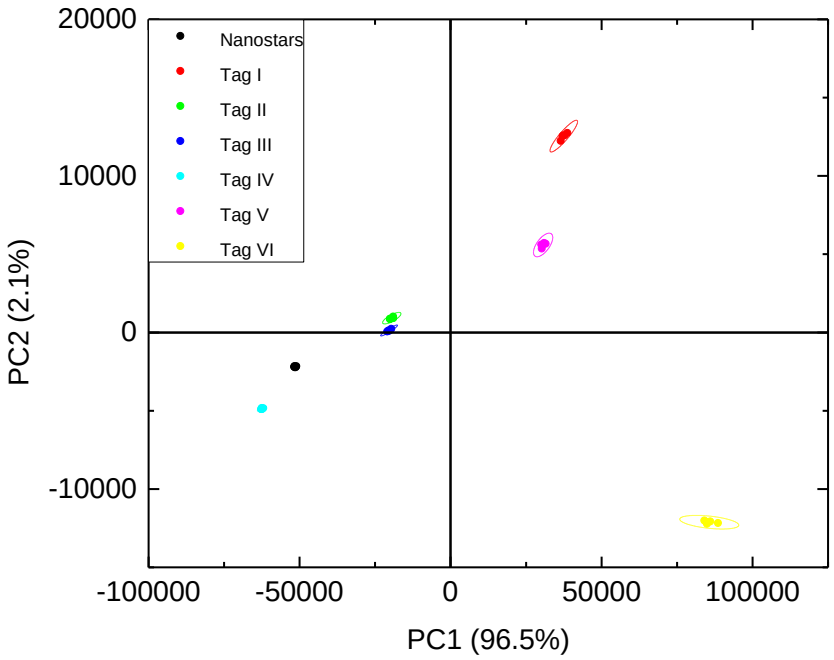

Figure 3.13 PCA score plot of the SERS spectra of the tag solutions and the AuNS.

3.5 Possibility to Increase Information Capacity

Thus far, the capacity of the tags is limited to the number of molecules that were used. One way to increase the information capacity is to vary the concentrations of the probe molecules in the tags. At different concentrations, SERS spectra are distinguishable due to different intensities. SERS spectra with higher concentrations of probe molecules tend to have greater intensities than those with lower concentrations of probe molecules. By utilizing a variety of probe molecule concentrations, the same number of probe molecule combinations can lead to a greater amount of tag combinations.

To test this, we studied Tag I and varied the concentration of MG. Four new tags were created using the original concentration of 100 μM as well as concentrations of 50

μM, 25 μM, and 0 μM. These tags were dubbed Tag I-A, Tag I-B, Tag I-C, and Tag I-D. Since MG was absent from Tag I-D it can be considered to be a different tag. Table 3.2 shows the binary encoding of each of these tags.

Table 3.2 Encoding of the four variants of Tag I with different concentrations of MG.

	4-MBA	R6G	MB	CV	Melamine	4-ATP	4-MPy	Ethanol	MG	
Tag I-A (Tag I)	1	0	0	0	1	0	1	1	1	279
Tag I-B	1	0	0	0	1	0	1	1	0.5	
Tag I-C	1	0	0	0	1	0	1	1	0.25	
Tag I-D	1	0	0	0	1	0	1	1	0	278

SERS spectra of the tags were measured and compared to the AuNS solution with no added probe molecules. Compared to the AuNS solution, the tags with MG had peaks that matched with the spectra of MG at 1172 cm^{-1} and 1398 cm^{-1}. SERS spectra of the five samples used in this study were acquired and the PCA score plot is shown in Figure 3.14. The relatively large confidence intervals represented by the Tag I-B and Tag I-C solutions may be due to the aggregation of AuNS in colloidal solutions caused by destabilization by the probe molecules. The relative locations of Tag I-D and the AuNS on the PCA plot are further away than the other three tags. This is due to the different chemicals that were added to the solutions. The AuNS had no added probe molecules and Tag I-D did not contain MG, which led to their separation from the other tags.

Based on the results of this study, concentration variety may be used to increase the information storage capacity of the tags. By adding a variety of probe molecule concentrations, the number of possible tag combinations can be greatly increased, which

allows for a larger quantity of unique tags to be fabricated. More unique tags means that the information storage capacity of the tags can be increased without using more probe molecules.

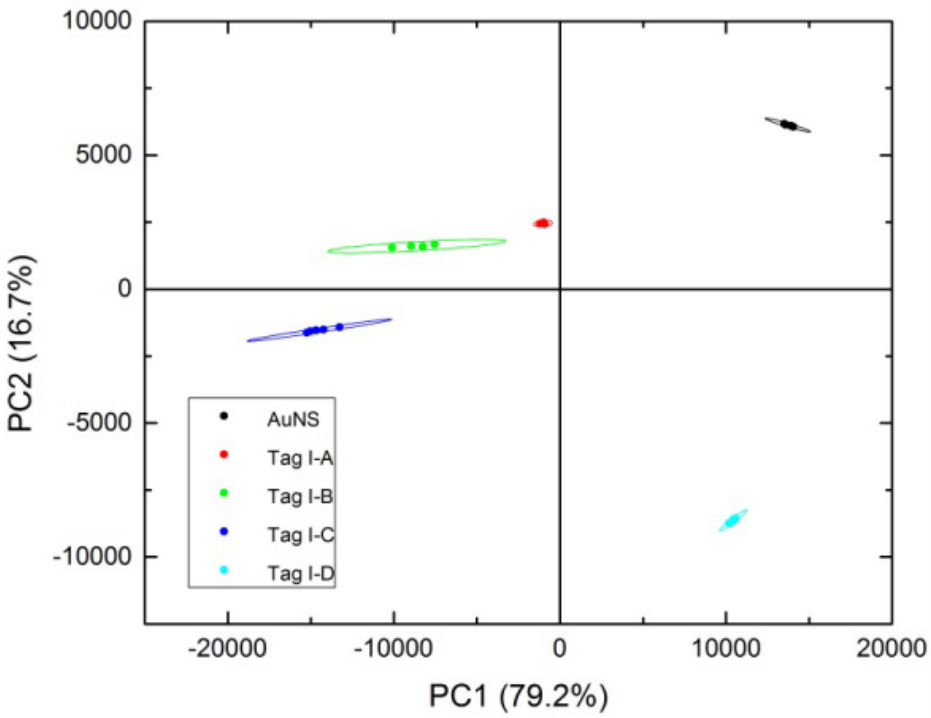

Figure 3.14 PCA score plot of the SERS spectra of the variants of Tag I with different MG concentrations.

3.6 Reproducibility and Stability Measurements

In order to be used as an effective anti-counterfeiting method, the tags must be able to be reproduced. To study the reproducibility, two tags were used, Tags IX and X. Two batches of AuNS, AuNS1 and AuNS2, were synthesized and combined with the tag solutions, resulting in four tags. The four tags were named AuNS1-TagIX, AuNS1-TagX, AuNS2-TagIX, and AuNS2-TagX. Table 3.3 shows the codes for these tags.

Table 3.3 Coding table for Tags IX and X used for reproducibility and stability measurements.

	4-MBA	R6G	MB	CV	Melamine	4-ATP	4-MPy	Ethanol	MG	
Tag IX	0	1	0	0	0	0	0	0	0	128
Tag X	0	1	1	0	0	1	0	0	0	200

The day that the samples were created, their SERS spectra were measured. After PCA analysis, the confidence intervals for Tags IX and X were separated and the different batches of AuNS could not be separated. The PCA plot for this measurement is shown in Figure 3.15. Since the AuNS batches could not be separated and the tag solutions could be separated, the tags were shown to be reproducible on that day that they were fabricated.

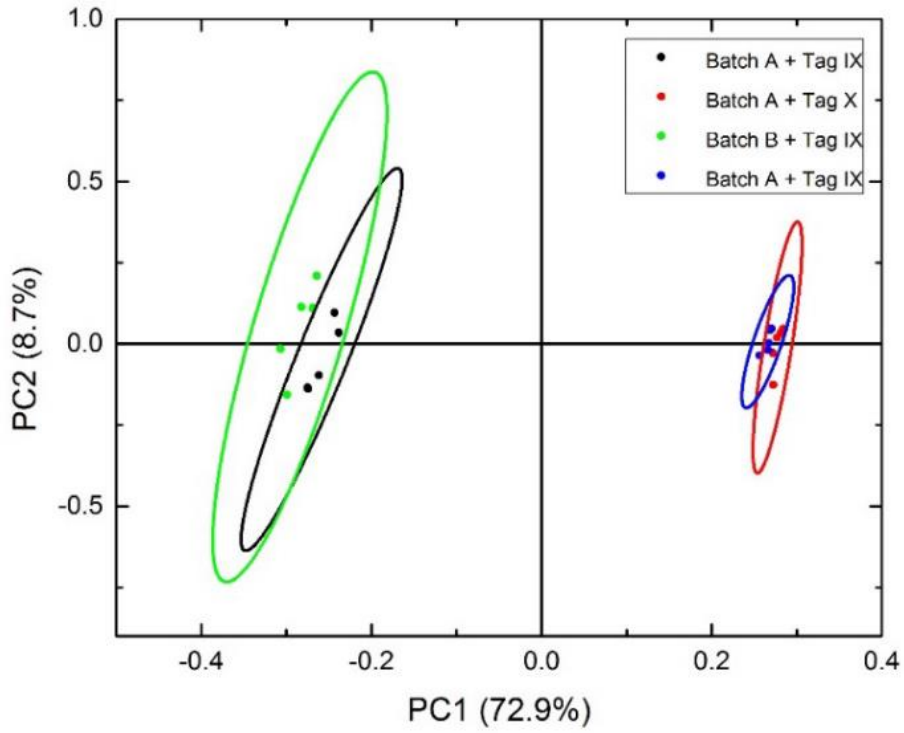

Figure 3.15 PCA score plot for the SERS spectra of Tags IX and X using the two different batches of AuNS on the day of fabrication.

When the SERS spectra of the samples were analyzed after day one, the confidence interval ellipses for the tag solutions were able to be separated. This means that beyond one day, the tags are able to be identified as the same, even though they were on day one. This may be due to aggregation of the AuNS or desorption of the probe molecules from the AuNS surface. Further improvements are necessary to increase the stability of the tag solutions so that they may be applicable in industrial settings.

CHAPTER FOUR

4 Conclusions and Future Work

This research has shown that there is potential to use SERS and AuNS in anti-counterfeiting applications. AuNS in combination with a system of various probe molecules were shown to be an effective technique for encoding molecular information. These tags were able to be differentiated using PCA. Through this research, a method has been introduced and examined for using SERS to fabricate anti-counterfeiting tags and examined methods of increasing their information capacity. These tags are discreet and difficult for counterfeiters to duplicate without a technical knowledge of the tag creation process, making them an ideal anti-counterfeiting technique.

In the future, more effort will be needed to refine this technique so that it is a suitable method to prevent counterfeiting. These tags currently have a limited capacity to store information and poor long-term stability in solution. A technique for using the portable Raman spectrometer and PCA software needs to be developed before the tags can be implemented in commercial settings. To improve these issues, the SERS enhancement of the AuNS needs to be addressed and improved as well as using a larger selection of probe molecules at various concentrations. Transferring the tags into a solid media should be considered to combat the stability issue and additional software should be developed that easily acquires the necessary spectra and processes them using PCA. With these issues addressed, these tags are a viable method to enhance security measures and prevent counterfeiting.

5 References

1. Bian, X.; Wang, K.-Y.; Smith, A.; Yannopoulou, N., New insights into unethical counterfeit consumption. *Journal of Business Research* **2016,** *69* (10), 4249-4258.
2. Kaczmarek, A. M.; Liu, Y.-Y.; Wang, C.; Laforce, B.; Vincze, L.; Van Der Voort, P.; Van Hecke, K.; Van Deun, R., Lanthanide "Chameleon" Multistage Anti-Counterfeit Materials. *Advanced Functional Materials* **2017,** *27* (20), 1700258.
3. Ren, W.; Lin, G.; Clarke, C.; Zhou, J.; Jin, D., Optical Nanomaterials and Enabling Technologies for High-Security-Level Anticounterfeiting. *Advanced Materials n/a* (n/a), 1901430.
4. Dégardin, K.; Roggo, Y.; Margot, P., Understanding and fighting the medicine counterfeit market. *Journal of Pharmaceutical and Biomedical Analysis* **2014,** *87*, 167-175.
5. Pecht, M.; Tiku, S., Bogus: electronic manufacturing and consumers confront a rising tide of counterfeit electronics. *IEEE Spectrum* **2006,** *43* (5), 37-46.
6. DiMase, D.; Collier, Z. A.; Carlson, J.; Gray Jr., R. B.; Linkov, I., Traceability and Risk Analysis Strategies for Addressing Counterfeit Electronics in Supply Chains for Complex Systems. *Risk Analysis* **2016,** *36* (10), 1834-1843.
7. Wang, Y.; Bai, N.; Yang, J.; Liu, Z.; Li, G.; Cai, M.; Zhao, L.; Zhang, Y.; Zhang, J.; Li, C.; Zhou, Y.; Guo, C. F., Silver nanowires for anti-counterfeiting. *Journal of Materiomics* **2020,** *6* (1), 152-157.
8. Kalytchuk, S.; Wang, Y.; Poláková, K.; Zbořil, R., Carbon Dot Fluorescence-Lifetime-Encoded Anti-Counterfeiting. *ACS Applied Materials & Interfaces* **2018,** *10* (35), 29902-29908.
9. Bhagavantam, S., Chandrasekhara Venkata Raman, 1888-1970. *Biographical Memoirs of Fellows of the Royal Society* **1971,** *17*, 564-592.
10. Pilot, R.; Signorini, R.; Durante, C.; Orian, L.; Bhamidipati, M.; Fabris, L., A Review on Surface-Enhanced Raman Scattering. *Biosensors-Basel* **2019,** *9* (2).
11. Kneipp, K.; Wang, Y.; Kneipp, H.; Perelman, L. T.; Itzkan, I.; Dasari, R. R.; Feld, M. S., Single Molecule Detection Using Surface-Enhanced Raman Scattering (SERS). *Physical Review Letters* **1997,** *78* (9), 1667-1670.
12. Ding, S.-Y.; Yi, J.; Li, J.-F.; Ren, B.; Wu, D.-Y.; Panneerselvam, R.; Tian, Z.-Q., Nanostructure-based plasmon-enhanced Raman spectroscopy for surface analysis of materials. *Nature Reviews Materials* **2016,** *1* (6), 16021.
13. Liu, Y.; Lee, Y. H.; Lee, M. R.; Yang, Y.; Ling, X. Y., Flexible Three-Dimensional Anticounterfeiting Plasmonic Security Labels: Utilizing Z-Axis-Dependent SERS Readouts to Encode Multilayered Molecular Information. *ACS Photonics* **2017,** *4* (10), 2529-2536.
14. Cui, Q.; Xia, B.; Mitzscherling, S.; Masic, A.; Li, L.; Bargheer, M.; Möhwald, H., Preparation of gold nanostars and their study in selective catalytic reactions. *Colloids and Surfaces A: Physicochemical and Engineering Aspects* **2015,** *465*, 20-25.
15. Ndokoye, P.; Li, X.; Zhao, Q.; Li, T.; Tade, M. O.; Liu, S., Gold nanostars: Benzyldimethylammonium chloride-assisted synthesis, plasmon tuning, SERS and catalytic activity. *Journal of Colloid and Interface Science* **2016,** *462*, 341-350.

16. Wang, S.; Huang, P.; Nie, L.; Xing, R.; Liu, D.; Wang, Z.; Lin, J.; Chen, S.; Niu, G.; Lu, G.; Chen, X., Single Continuous Wave Laser Induced Photodynamic/Plasmonic Photothermal Therapy Using Photosensitizer-Functionalized Gold Nanostars. *Advanced Materials* **2013,** *25* (22), 3055-3061.
17. Yuan, H.; Fales, A. M.; Vo-Dinh, T., TAT Peptide-Functionalized Gold Nanostars: Enhanced Intracellular Delivery and Efficient NIR Photothermal Therapy Using Ultralow Irradiance. *Journal of the American Chemical Society* **2012,** *134* (28), 11358-11361.
18. Dondapati, S. K.; Sau, T. K.; Hrelescu, C.; Klar, T. A.; Stefani, F. D.; Feldmann, J., Label-free Biosensing Based on Single Gold Nanostars as Plasmonic Transducers. *ACS Nano* **2010,** *4* (11), 6318-6322.
19. Verma, M. S.; Chen, P. Z.; Jones, L.; Gu, F. X., Branching and size of CTAB-coated gold nanostars control the colorimetric detection of bacteria. *RSC Advances* **2014,** *4* (21), 10660-10668.
20. Rodríguez-Lorenzo, L.; Krpetic, Z.; Barbosa, S.; Alvarez-Puebla, R. A.; Liz-Marzán, L. M.; Prior, I. A.; Brust, M., Intracellular mapping with SERS-encoded gold nanostars. *Integrative Biology* **2011,** *3* (9), 922-926.
21. Yuan, H.; Khoury, C. G.; Wilson, C. M.; Grant, G. A.; Bennett, A. J.; Vo-Dinh, T., In vivo particle tracking and photothermal ablation using plasmon-resonant gold nanostars. *Nanomedicine: Nanotechnology, Biology and Medicine* **2012,** *8* (8), 1355-1363.
22. Meng, X.; Baride, A.; Jiang, C., Ligand Controlled Morphology Evolution of Active Intermediates for the Syntheses of Gold Nanostars. *Langmuir* **2016,** *32* (26), 6674-6681.
23. Meng, X.; Dyer, J.; Huo, Y.; Jiang, C., Greater SERS Activity of Ligand-Stabilized Gold Nanostars with Sharp Branches. *Langmuir* **2020,** *36* (13), 3558-3564.
24. Frens, G., Particle size and sol stability in metal colloids. *Kolloid-Zeitschrift und Zeitschrift für Polymere* **1972,** *250* (7), 736-741.
25. Frens, G., Controlled Nucleation for the Regulation of the Particle Size in Monodisperse Gold Suspensions. *Nature Physical Science* **1973,** *241* (105), 20-22.